Plasmon-Modulated Light Scattering from Gold Nanocrystal-Decorated Hollow Mesoporous Silica Microspheres

Manda Xiao, Huanjun Chen, Tian Ming, Lei Shao, and Jianfang Wang*

Department of Physics, The Chinese University of Hong Kong, Shatin, Hong Kong SAR, China

ARTICLE

ABSTRACT Localized surface plasmon resonances of noble metal nanocrystals are powerful in enhancing a variety of linear and nonlinear optical signals and photorelated processes. Here we demonstrate the plasmonic enhancement of the light scattering from hollow mesoporous silica microspheres by attaching a dense layer of gold nanocrystals onto the outer surface of the microspheres. The attachment of gold nanocrystals induces both the shift and intensity increase in the resonant scattering peaks of the microspheres. The spectral region of the resonant scattering enhancement can be controlled by using gold nanocrystals with different plasmon resonance wavelengths. The spectral region of the enhancement is independent of the microsphere diameter. The scattering enhancement factor ranges from 20 to 130, depending on the plasmonic properties and surface coverage of the attached gold nanocrystals. The systematic evolution of the scattering spectra of the individual microspheres is also revealed by chemically etching away the attached gold nanocrystals gradually.

KEYWORDS: gold nanorods · hollow microspheres · mesoporous silica · plasmon resonance · scattering

The localized surface plasmon resonances of noble metal nanocrystals and their assemblies can greatly concentrate light to the regions close to the metal surfaces and in the gaps between metal nanocrystals. The plasmon-induced concentration of light has been used widely for enhancing a variety of optical signals, including Raman,[1,2] fluorescence,[3] two-photon-excited photoluminescence,[4] photopolymerization,[5,6] high-harmonic generation,[7] and light absorption for solar energy harvesting.[8,9] For example, single-molecule fluorescence measurements have shown fluorescence intensity enhancements of up to 1340 for fluorescent molecules that are located in the gap region of bowtie gold nanoantennas.[3] A reduction of the threshold of the laser pulse intensity by at least 2 orders of magnitude for high-harmonic generation has been demonstrated on bowtie gold nanostructure arrays.[7]

Light scattering has been a powerful technique in areas ranging from life science, process analytics, remote sensing, and astrophysics. It has been widely employed for measuring the size, shape, and refractive index of biological particles, macromolecules, colloids, aerosols, geological, and astrophysical particles. For example, cells are building blocks of biological organisms. The structural and compositional changes inside cells are usually indicators of dysplasia or carcinoma.[10] Many efforts have been made to detect the small changes in cellular physiology, which are associated with cell functions, including the measurements of the local pH, intra- or extra-cellular potential, fluorescence, and refractive index. Among these techniques, light scattering spectroscopy is a noninvasive detection method based on the elastic scattering signals from cells.[11,12] Early detection of cancer in epithelial cells has been demonstrated by analyzing the nuclear size distribution from the backscattered light signals of the cells.[13,14] Light scattering signals have also been utilized to reconstruct the images of the subcellular regions inside cells.[10,11] Despite these successes, the light signals scattered from cells are often disturbed by the signals from the extracellular environment, because of the small difference in the refractive index between cells and their environment.[15] If the scattering signals from individual cells can be enhanced relative to their extracellular environment, the cell metabolic activities and malfunctioning behaviors can then be observed with light scattering in more details or even monitored as a function of time.

The plasmon-induced concentration of light onto the regions adjacent to metal nanocrystals can in principle also be utilized for enhancing the light scattering from dielectric particles. In contrast to two previous works, where dielectric nanoparticles are placed close to the metal surface and in

*Address correspondence to jfwang@phy.cuhk.edu.hk.

Received for review July 28, 2010 and accepted October 05, 2010.

Published online October 12, 2010.
10.1021/nn101804v

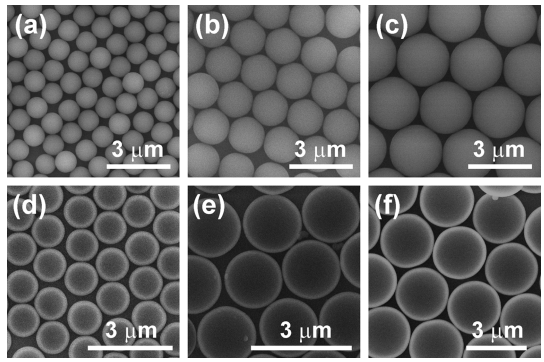

Figure 1. (a−c) SEM images of the PS microspheres with average diameters of 1.04, 1.73, and 2.53 μm, respectively. (d−f) SEM images of the HMSMSs with average outer diameters of 1.22, 1.80, and 2.72 μm, respectively.

the gap between neighboring metal nanocrystals, respectively,[16,17] we demonstrate here the selective enhancement of the elastic light scattering signals from hollow mesoporous silica microspheres (HMSMSs) by taking advantage of the localized plasmon resonances of Au nanocrystals. The coating of a dense layer of Au nanocrystals onto HMSMSs induces both the shift and intensity increase in the resonant scattering peaks of the individual microspheres. The scattering spectrum of the Au nanocrystal-decorated HMSMS is clearly not the simple superposition of the scattering spectra from the two constituents. The spectral region of the scattering intensity enhancement is controllable by using Au nanocrystals with different surface plasmon resonance wavelengths (SPRWs), irrespective of the microsphere diameter. The scattering intensity enhancement increases as the coated Au nanocrystals become larger. The plasmon-modulated scattering behavior is further revealed by chemically etching away the coated Au nanocrystals. We believe that our results might open up the possibilities for the real-time monitoring of the functions and activities of live cells by decorating plasmonic metal nanocrystals onto cell membranes.

RESULTS AND DISCUSSION

The HMSMSs were produced by growing mesostructured silica shells on preprepared polystyrene (PS) core microspheres. The PS cores were made through dispersion polymerization of styrene in an ethanol−water medium, as described previously.[18] Their diameters were adjusted by varying the chemical composition in the reaction mixture. All of the obtained PS microspheres have very narrow size distributions. Three PS microsphere samples were used in this study. Their diameters are 1.04 ± 0.01, 1.73 ± 0.02, and 2.53 ± 0.03 μm, respectively (Figure 1a−c). The coating of mesostructured silica shells on the PS microspheres was realized through the hydrolysis and condensation of tetraethyl orthosilicate (TEOS) in the presence of cetyltrimethylammonium bromide (CTAB) as a mesostructure-directing agent according to a previously described procedure.[19] The coating of a uniform silica layer in the absence of the surfactant was found to be difficult. Calcination of the core−shell microspheres produced the HMSMSs, which have uniform overall diameters, as revealed by scanning electron microscopy (SEM) imaging (Figure 1d−f and Supporting Information Figure S1a,c,e). The shell thickness was measured and the mesoporosity were corroborated by transmission electron microscopy (TEM) imaging on the deliberately crushed HMSMSs (Supporting Information Figures S1b,d,f, and S2). The average overall diameters and shell thicknesses of the three HMSMS samples used in our experiments are 1.22 ± 0.04 μm/108 ± 3 nm, 1.80 ± 0.02 μm/77 ± 4 nm, and 2.72 ± 0.04 μm/134 ± 6 nm, respectively. The shell thickness is highly uniform for each HMSMS and among different HMSMSs. In addition, the refractive index of the mesoporous silica shell is estimated to be 1.39 from the measured pore volume[19] when the HMSMSs are immersed in water. The index ratio of the shell to water is calculated to be 1.05, which is in the range of 1.02−1.10 for biologically relevant structures.[10] The appropriate refractive index possessed by the shell might therefore allow our HMSMSs to be employed for modeling cells.

The scattering properties of the HMSMSs were investigated using the dark-field technique.[20] For the optical measurements, the aqueous HMSMS dispersion was deposited in a sandwich structure made of two glass slides and one poly(dimethylsiloxane) (PDMS) block. A square hole was opened at the center of the PDMS block. The HMSMS sample was maintained in an aqueous environment throughout the optical measurement. Each HMSMS appears as a bright spot on the scattering image (Figure S3, Supporting Information). The scattering spectra from the different HMSMSs with the same average size nearly overlap with each other when they are plotted together without intensity normalization (Figure S4, Supporting Information). The nearly identical scattering spectra over the entire spectral range of detection from 400 to 900 nm suggest that the HMSMSs are very uniform in size in terms of their overall diameters and shell thicknesses. Figure 2 shows the representative scattering spectra of the individual HMSMSs for the three differently sized samples. For each spectrum, a series of resonant scattering peaks are clearly observable. As the diameter of the HMSMS is increased, more resonant scattering peaks are observed in the spectral range of detection. Similar scattering features have been previously observed in mucosal tissue.[13] Because the HMSMSs are immersed in water during the scattering measurements, the small difference between the refractive indices of water and the mesoporous silica shell makes the HMSMSs good candidates for modeling the scattering behaviors of biological structures. Mie theory extended to core−multishell structures based on the recursion algorithm[21] was utilized to simulate the scattering spectra of the individual

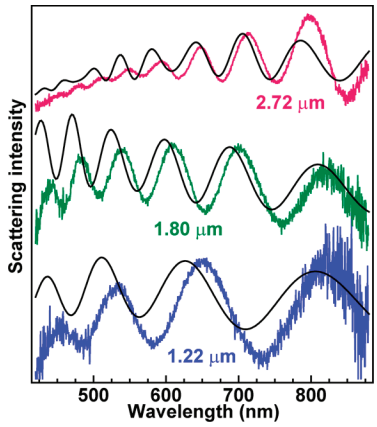

Figure 2. Single-particle scattering spectra of the three differently sized HMSMS samples. The black curves are obtained from the calculations based on Mie theory.

HMSMSs (see Supporting Information for the calculation details). The calculated scattering spectra (Figure 2, black curves) are in good agreement with the experimental ones. This result indicates that the light signal collected above the individual HMSMSs from the solid angle of 30°, which is determined by the numerical aperture of the objective (Figure S5, Supporting Information), originates from the resonant scattering in the HMSMSs. The slight red shifts of the scattering peaks on the measured spectra relative to those on the calculated spectra are believed to result from the use of glass slides to support the HMSMSs during the scattering measurements, while the HMSMSs are assumed to be surrounded uniformly with water in the calculations. The inverses of the peak wavelengths are found to be nearly equally spaced. The spacing between the inverses of the neighboring peak wavelengths is inversely proportional to the diameter of the HMSMS. These results are similar to those of Fabry−Perot interferometers, where the inverses of the reflection peak wavelengths are equally spaced, and the spacing is inversely proportional to the distance between the two mirrors. In addition, gas bubbles and dielectric microspheres have also been approximated as Fabry−Perot interferometers made of two spherical mirrors in previous backscattering studies.[22,23] Taking these together, we therefore believe that the resonant scattering peaks observed on the HMSMSs can be essentially ascribed to Fabry−Perot interference. The resonant peaks on the scattering spectra detected under our geometrical measurement configuration mainly result from the constructive interference between the light directly scattered from the microsphere and that traveling a round trip inside the microsphere. We also measured the scattering spectra of the PS microspheres and uncalcined PS core−mesostructured silica shell structures (Supporting Information Figure S6). The overall scattering intensities of both structures are 20−30 times larger than those of the HMSMSs. In addition, the resonant scattering peaks of the PS microspheres are barely resolved. The growth of the mesostructured silica shell makes the resonant scattering peaks distinguishable, and the removal of the PS core generates the sharpest scattering peaks.

Gold nanocrystals, including nanorods and nanospheres, were chosen for the enhancement of the resonant scattering from the HMSMSs, because their sizes and therefore their SPRWs can be readily controlled synthetically. The preparation of Au nanorods employed a seed-mediated method in conjunction with the shortening through anisotropic oxidation.[24,25] The preparation of Au nanospheres followed Frens' method.[26] To facilitate the deposition of the Au nanocrystals onto the HMSMSs, the nanocrystals were functionalized with thiol-terminated methoxypoly(ethylene glycol) (mPEG-SH) according to a reported method.[27] Figure 3 panels a, d, g, and j show the TEM images of the PEGylated Au nanosphere and three representative PEGylated Au nanorod samples. The Au nanosphere sample has an average diameter of 27 ± 3 nm with an ensemble SPRW of 526 nm (Figure 3c, green curve), and the three nanorod samples have average diameters/lengths of 21 ± 2/47 ± 5, 19 ± 2/64 ± 6, and 19 ± 1/78 ± 6 nm, with ensemble longitudinal SPRWs of 622, 756, and 853 nm (Figure 3f,i,l, green curves), respectively. The PEGylated Au nanocrystals were adsorbed onto the HMSMSs simply by mixing them together and subjecting the mixture solution to vigorous shaking for 10 min.

As an example, Figure 3 panels b,e,h, and k show the SEM images of the 1.80-μm HMSMSs decorated with the four Au nanocrystal samples. The large-area SEM images of the same samples are shown in Figure S7 in Supporting Information. The Au nanocrystals are uniformly distributed on the surface of each HMSMS. The numbers of the Au nanocrystals are estimated to be 4500, 4400, 4300, and 4100 per HMSMS, which correspond to surface area coverage percentages of 32%, 42%, 51%, and 59%, respectively (see Experimental Methods for how to estimate the surface area coverage percentage). The uniform deposition of the Au nanocrystals on the HMSMSs is believed to arise from the interaction between the grafted polymer chains and the silica surface.[27] An intimate contact between the polymer chains and the silica surface can reduce the interfacial energy between the polymer chains and water. Compared to the ensemble extinction spectra of the PEGylated Au nanocrystals, those of the Au nanocrystal-decorated HMSMSs exhibit both red shifts and considerable peak broadening (Figure 3 panels c, f, i, and l, red curves). The red shifts and peak broadening in the plasmon resonance are ascribed to the increase in the refractive index of the surrounding medium of each Au nanocrystal and the plasmon resonance coupling among neighboring Au nanocrystals when they are adsorbed on the HMSMSs. The extent of the peak broadening increases as the Au nanocrystals become larger, reflecting the increase in the plasmon coupling strength. The increased plasmon coupling strength is ascribed to the re-

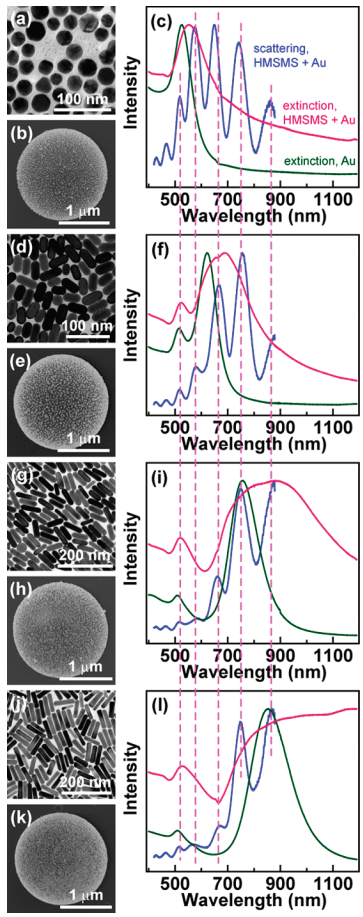

Figure 3. (a−c) The HMSMSs decorated with the Au nanospheres that have a SPRW of 526 nm: (a) TEM image of the PEGylated Au nanospheres; (b) SEM image of a single HMSMS decorated with a dense layer of the Au nanospheres; (c) extinction spectra of the PEGylated Au nanosphere sample (green) and the Au nanosphere-decorated HMSMS sample (red), and the scattering spectrum from a single HMSMS decorated with the Au nanospheres (blue). (d−f) Corresponding data for the HMSMSs decorated with the Au nanorods that have a longitudinal SPRW of 622 nm. (g−i) Corresponding data for the HMSMSs decorated with the Au nanorods that have a longitudinal SPRW of 756 nm. (j−l) Corresponding data for the HMSMSs decorated with the Au nanorods that have a longitudinal SPRW of 853 nm. The average diameter is 1.80 μm for all of the HMSMS samples. The spectra are vertically shifted for clarity. The vertical dashed lines indicate the resonant scattering peaks of the HMSMSs decorated with the differently sized Au nanocrystals.

duction in the average spacing between the Au nanocrystals on the HMSMSs, because the surface area coverage of the Au nanocrystals is increased as the nanocrystal size gets larger.

The scattering properties of the HMSMSs are drastically altered after the decoration of the Au nanocrystals (Figure 3 panels c, f, i, and l, blue curves). The resonant scattering from the individual HMSMSs is found to be selectively enhanced. As the ensemble SPRW of the adsorbed Au nanocrystals gets longer, the resonant scattering peaks in the shorter-wavelength region become weaker, and those in the longer-wavelength region becomes stronger. The overall enhancement region nearly overlaps with the ensemble plasmon resonance peak. As a result, the resonant scattering enhancement can be tailored from the visible to near-infrared spectral region by using Au nanocrystals with different SPRWs. The enhancement region caused by the Au nanospheres appears red-shifted in comparison to the ensemble plasmon peak. This can be ascribed to two factors. One is that the scattering peak of the Au nanospheres is red-shifted in comparison to the extinction peak (Figure S8, Supporting Information), as shown by finite-difference time-domain calculations (see Supporting Information for the calculation details). The other is the relatively small enhancement factors caused by the Au nanospheres (see below). The enhancement region seems to cover a wide spectral range. In fact, the maximum enhancement region for the Au nanospheres is in the range of 560−640 nm. The spectrally selective enhancement of the resonant scattering can be understood by considering the light concentration capability of plasmonic Au nanocrystals. When the Au nanocrystals are adsorbed on the surface of the HMSMSs, the excitation light in the spectral region of the plasmon resonance is concentrated to the spatial region close to the Au nanocrystals and coupled into the HMSMSs. The light travels a round trip inside the HMSMSs and interferes constructively with the light directly scattered from the Au nanocrystals, producing the resonant peaks on the far-field scattering spectra. We have tried to use Mie theory to simulate the scattering spectra of the Au nanocrystal-decorated HMSMSs, but have so far been unsuccessful. The main difficulty lies in that the dielectric function of the adsorbed Au nanocrystal layer cannot be well-defined. In addition, the scattering spectra acquired from the different microspheres for the same Au nanocrystal-decorated HMSMS sample are very similar to each other in terms of both the scattering intensity and spectral shape (Supporting Information Figure S9). This result suggests that the overall coating of the Au nanocrystals is very uniform on the different HMSMSs with the same diameter.

We further demonstrated that the selective enhancement of the resonant scattering by the adsorbed Au nanocrystals is independent of the diameter of the HMSMSs. Figure 4 panels a, c, and e show the representative SEM images of the 1.22-, 1.80-, and 2.72-μm HMSMSs decorated with the same Au nanorod sample that have a longitudinal SPRW of 708 nm (Figure 4 panels b, d, and f, green curves), respectively. The three Au nanorod-decorated HMSMS samples exhibit very similar extinction spectra (Figure 4 panels b, d, and f, red curves), suggesting that the distribution of the Au nanorods on the HMSMSs is insensitive to the surface curvature. This is also consistent with the estimated surface area coverage percentages, which are 48%, 48%, and 46% for the 1.22-, 1.80-, and 2.72-μm HMSMSs, respectively. Although the scattering signatures have been shown to be highly dependent on the size of the HMSMSs, only the resonant scattering peaks close to

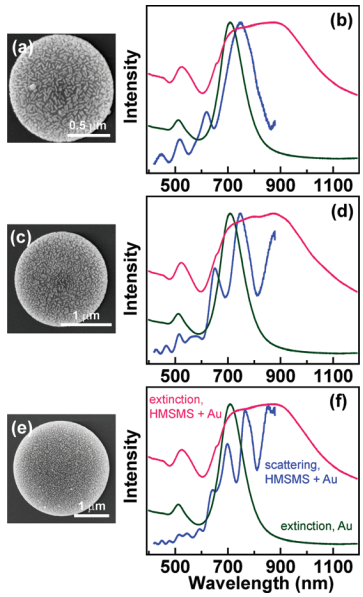

Figure 4. Comparison of the resonant scattering among the differently sized HMSMSs that are coated with the same Au nanorod sample with a longitudinal SPRW of 708 nm: (a, b) 1.22-μm HMSMSs; (c, d) 1.80-μm HMSMSs; (e, f) 2.72-μm HMSMSs. Shown at the left side are the SEM images. The extinction and scattering spectra are shown at the right side. The green curves are the extinction spectra of the PEGylated Au nanorod sample. The red curves represent the extinction spectra of the Au nanorod-decorated HMSMS samples. The blue curves are the scattering spectra of the individual Au nanorod-decorated HMSMSs. The spectra are vertically shifted for clarity.

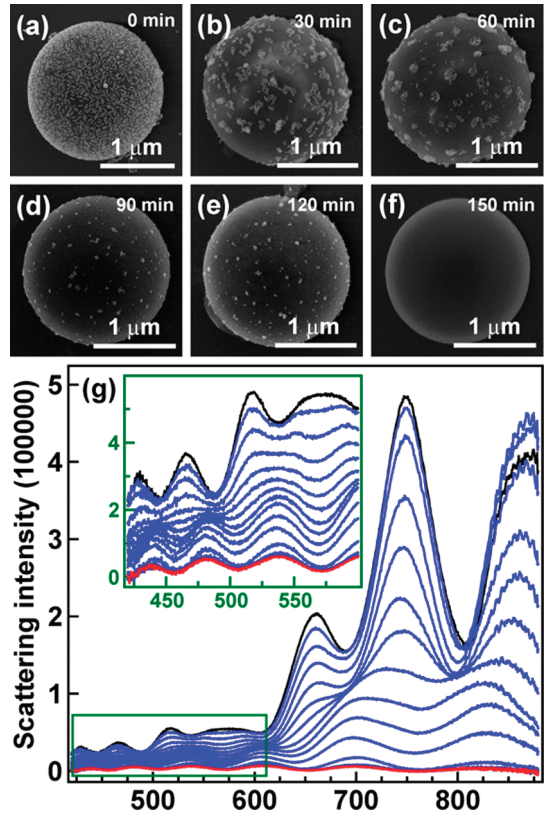

Figure 5. Real-time monitoring of the evolution of the scattering spectra during chemical etching. (a−f) SEM images of the 1.80-μm, Au nanorod-decorated HMSMSs undergoing the chemical etching for a varying period of time. The longitudinal SPRW of the Au nanorod sample is 756 nm. (g) Scattering spectra of a single HMSMS recorded every 10 min during the etching. The black and red curves correspond to the scattering spectra taken at the start and end of the etching. The inset shows the spectral region from 420 to 600 nm in a magnified view.

the plasmon resonance are strongly enhanced (Figure 4 panels b, d, and f, blue curves). Therefore the resonant scattering enhancement is independent of the size of the original particles. Such plasmon-modulated scattering enhancements can be utilized to adjust scattering signals to the target wavelength region by using noble metal nanocrystals with different SPRWs.

The scattering enhancement factors and spectral shifts arising from the plasmon resonance were finally ascertained by gradually etching away the Au nanocrystals adsorbed on the HMSMSs through an oxidation reaction with H_2O_2 as the oxidizing agent.[28] The scattering spectra from the individual HMSMSs were recorded as a function of time during the etching process. SEM imaging was also performed on the Au nanocrystal-decorated HMSMSs that were deposited on silicon substrates and immersed in the H_2O_2 solution for varying periods of time. The SEM images (Figure 5a−f) indicate that the chemical etching process lasts for ~150 min. A careful inspection of the SEM images reveals that the etching involves both the detachment and oxidation of the Au nanocrystals. The detachment can be attributed to the oxidation of the thiol group, which leads to the cleavage of the sulfur−gold bond and therefore the separation of the mPEG polymer chains from the Au nanocrystals. The SEM imaging also shows that the Au nanocrystals are aggregated together to form clusters on the surface of each HMSMS.

The Au nanocrystal aggregation is believed to be caused by the drying process after the silicon substrate carrying the HMSMSs was pulled out of the etching solution. The oxidation of Au nanocrystals with H_2O_2 has been demonstrated previously.[28] During the oxidation, the Au nanocrystals are observed to first shrink in size gradually and finally completely dissolved.

Figure 5g shows the evolution of the scattering spectra of a 1.80-μm HMSMS decorated with the Au nanorods with a longitudinal SPRW of 756 nm. The resonant scattering peaks decrease rapidly in intensity when the Au nanorods are detached away from the HMSMS. The intensity decrease is accompanied with a small blue shift in the resonant scattering peaks. This trend is also observed on the 1.80-μm HMSMSs decorated with the Au nanocrystals that have other SPRWs (Supporting Information Figure S10a−c). After the Au nanocrystals are completely etched away, the scattering spectra of the HMSMSs return to those of the corresponding bare HMSMSs (Supporting Information Figure S10d). Moreover, the scattering spectra of the HMSMSs obtained after the complete etching of the Au nanocrystals are nearly the same as those of the cor-

responding HMSMSs before the decoration of the Au nanocrystals (Supporting Information Figure S10e). These observations suggest that the HMSMSs are well preserved throughout the Au nanocrystal decoration and chemical etching processes.

The complete etching of the Au nanocrystals allows us to determine the scattering enhancement factor, which is calculated by taking the ratio between the intensity of the strongest resonance peak before the etching and that of the corresponding resonance peak after the etching. For the 1.80-μm HMSMSs decorated with the Au nanocrystals with SPRWs of 526, 622, 756, and 853 nm, the enhancement factors are determined to be 20, 77, 87, and 127, respectively. The enhancement factor is found to be in a direct correlation with the surface area coverage percentage of the Au nanocrystals on the 1.80-μm HMSMSs. On the other hand, the numbers of the Au nanocrystals on a single 1.80-μm HMSMS have been estimated to be 4500, 4400, 4300, and 4100 for the Au nanocrystals with SPRWs of 526, 622, 756, and 853 nm, respectively. Taking into account this fact suggests that the nanocrystal size and therefore the scattering cross section of the metal nanocrystal play a more important role in the resonant scattering enhancement.

The spectral shift of the resonant scattering peaks accompanying the scattering intensity enhancement is more clearly discernible by plotting together the normalized scattering spectra recorded before and after the etching (Figure 6). For example, for the 1.80-μm HMSMSs, the decoration of the Au nanocrystals with a SPRW of 756 nm causes the resonant scattering peaks at 438, 480, 538, 607, and 699 nm of the bare HMSMSs to red-shift by 28, 37, 32, 54, and 50 nm, respectively (Figure 6c). This spectral shift can be ascribed to the resonant scattering mode modification by the plasmon resonance of the adsorbed Au nanocrystals. The scattering of the adsorbed Au nanocrystals can change the phase and optical path of the light. In addition, the enhanced scattering signal in the selective spectral region cannot be attributed to a simple superposition of the scattering from both the HMSMS and the ensemble of the adsorbed Au nanocrystals. Otherwise, the scattering spectra from the Au nanocrystal-decorated HMSMSs will appear as an overlap of a series of weak peaks from the HMSMS with a much stronger, plasmon-induced peak of the ensemble of the Au nanocrystals. Furthermore, Figure 6 shows clearly that the overall scattering enhancement region red-shifts as the SPRW of the adsorbed Au nanocrystals becomes longer, corroborating the selective enhancement of the scattering from the HMSMSs.

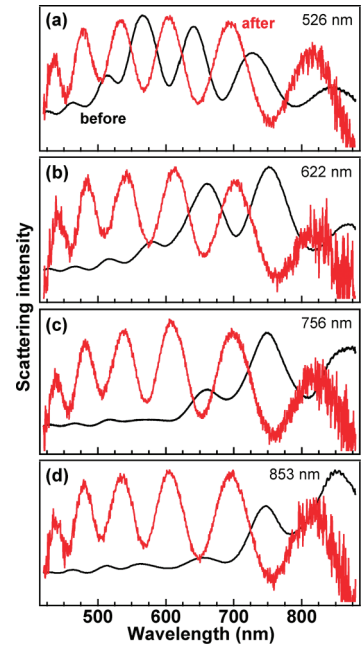

Figure 6. Normalized scattering spectra recorded on the HMSMS before (black) and after (red) the etching. The HMSMSs have an average diameter of 1.80 μm and are decorated with (a) the Au nanospheres with an ensemble SPRW of 526 nm, (b) the nanorods with a longitudinal SPRW of 622 nm, (c) the nanorods with a longitudinal SPRW of 756 nm, and (d) the nanorods with a longitudinal SPRW of 853 nm, respectively.

CONCLUSIONS

We have shown that the resonant scattering from the individual HMSMSs can be enhanced by the plasmon resonance of the Au nanocrystals that are adsorbed on the surface of the HMSMSs. The enhancement factor ranges from 20 to 130, depending on the plasmonic properties and surface coverage of the adsorbed Au nanocrystals. Moreover, the spectral region of the scattering enhancement can be controlled by the SPRW of the adsorbed Au nanocrystals. The resonant scattering peaks close to the plasmon resonance exhibit the strongest enhancement. These results will be useful for the use of the localized surface plasmons to concentrate light for improving the harvesting efficiency of the solar energy. Our approach may also open up possibilities for the real-time monitoring of the functions and metabolic activities of live cells by the use of localized surface plasmons to enhance the light scattering from the cells.

EXPERIMENTAL METHODS

Preparation of Monodisperse PS Microspheres. Monodisperse PS microspheres with different diameters were prepared by dispersion polymerization of styrene with poly(vinyl pyrrolidone) (PVP, M_W = 55000) as a steric stabilizer and 2,2′-azobis(2-methylpropionitrile) (AIBN) as a radical initiator in an ethanol−water medium. The reaction compositions for the preparation of the three differently sized PS microsphere samples are listed in Table 1. All of the chemicals, including styrene, PVP, AIBN, ethanol, and water, were added to a 250-mL, three-necked, round-bottom flask equipped with a reflux condenser and a nitrogen gas inlet. The air in the flask was replaced

TABLE 1. Reaction Compositions for the Preparation of the PS Microspheres

diameter (μm)	styrene (mL)	AIBN (g)	PVP (g)	ethanol (mL)	water (mL)
1.04	10	0.1	2.25	95	3
1.73	20	0.2	1.50	95	3
2.53	30	0.3	2.25	95	3

by a stream of nitrogen, and the mixture was kept under nitrogen until the polymerization was finished. The dispersion polymerization was carried out at 70 °C for 24 h, and the stirring rate was set at 120 rpm.

Preparation of HMSMSs. The reaction compositions for the coating of mesostructured silica on the PS microspheres are given in Table 2, where CTAB was employed as the structure-directing agent and TEOS was employed as the silica precursor. In a typical synthesis of the 1.8-μm HMSMSs, the 1.73-μm PS microsphere sample (0.96 g) was first dispersed in a mixture containing ethanol (60 mL), water (50 mL), and $NH_3 \cdot H_2O$ (0.8 mL, 28 wt %). A solution of CTAB (0.48 g) dissolved in a mixture containing water (8 mL) and ethanol (4 mL) was then added. After the mixture solution was stirred for 30 min, TEOS (0.86 mL) was quickly added, followed by stirring for 3 min. The mixture was thereafter kept undisturbed overnight. The product was collected by filtration and then calcined at 550 °C for 6 h with a ramp rate of 1 °C · min^{-1} to remove PS and CTAB templates.

Growth of Au Nanorods. The Au nanorods were grown using a seed-mediated method. The seed solution was prepared by adding a freshly prepared, ice-cold aqueous $NaBH_4$ solution (0.6 mL, 0.01 M) into an aqueous mixture solution made of $HAuCl_4$ (0.25 mL, 0.01 M) and CTAB (9.75 mL, 0.1 M). The resultant solution was mixed by rapid inversion for 2 min and then kept at room temperature for at least 2 h before use. The growth solution was made by first mixing together $HAuCl_4$ (2 mL, 0.01 M), $AgNO_3$ (0.4 mL, 0.01 M), and CTAB (40 mL, 0.1 M). A freshly prepared aqueous ascorbic acid solution (0.32 mL, 0.1 M) was then added, followed by the addition of an aqueous HCl solution (0.8 mL, 1.0 M). After the resultant solution was mixed by inversion, the seed solution (96 μL) was then added. The reaction mixture was subjected to gentle inversion for 10 s and then left undisturbed for at least 6 h. The as-grown Au nanorods have an ensemble longitudinal SPRW of 853 nm, and the particle concentration is estimated to be ~0.2 nM. The Au nanorods with longitudinal SPRWs of 756, 708, and 622 nm were prepared through anisotropic oxidation of the nanorod sample with a longitudinal SPRW of 853 nm. For oxidation, an aqueous solution (0.2 mL, 1.0 M) was added in the as-grown nanorod solution (10 mL), followed by bubbling O_2 into the mixture solution for 1 min. The mixture solution was then kept uncapped in an isothermal oven at 65 °C for 2−25 h. The longitudinal SPRW of the Au nanorods became shorter with the increase in the oxidation time. After oxidation, the Au nanorods were precipitated by centrifugation and then redispersed in aqueous CTAB solutions (0.1 M) at the same volume.

Growth of Au Nanospheres. The citrate-stabilized Au nanospheres were synthesized according to Frens' method. Typically, an aqueous trisodium citrate solution (3 mL, 0.01 g · mL^{-1}) was added to a boiling aqueous $HAuCl_4$ solution (150 mL, 0.25 mM). The mixture was kept boiling for 10 min and then cooled down naturally.

PEGylation of the Au Nanocrystals. For the Au nanorods capped with CTAB, excess CTAB was first removed to ensure successful PEGylation. Specifically, the as-grown Au nanorods in 0.1 M aqueous CTAB solutions (5 mL) were centrifuged at 6300*g* for 10 min and then redispersed in deionized water (5 mL). To this Au nanorod solution was added an aqueous mPEG-SH (M_W = 5000, Rapp Polymere GmbH, 0.25 mL, 1 mM for the polymer). The mixture was left undisturbed for 6 h. Excess mPEG-SH was removed by centrifugation at 6300*g* for 10 min. The Au nanorod precipitate was washed once with water (5 mL) by centrifugation at the same condition and then redispersed in water (1 mL) for further use. For the citrate-stabilized Au nanospheres, the aqueous mPEG-SH solution (0.25 mL, 1 mM) was added to the as-prepared nanosphere solution (20 mL). The mixture was left undisturbed for 6 h and then washed twice with water by centrifugation at 8000*g* for 10 min. The Au nanospheres were finally redispersed in water (1 mL).

Adsorption of the PEGylated Au Nanocrystals onto the HMSMSs. The PEGylated Au nanocrystals were washed with water and concentrated to ~1 nM. The concentrated nanocrystal solution (1 mL) was then mixed with the HMSMS dispersion (0.1 mL, 1 mg · mL^{-1}). After the mixture was vigorously shaken with a vortex mixer for 10 min, the Au nanocrystal-decorated HMSMSs were collected by centrifugation and washed twice with water to remove the excess nanocrystals in the solution. The surface area coverage percentage of the adsorbed Au nanocrystals was estimated according to the total number of the adsorbed Au nanocrystals and the nanocrystal size. The number of the adsorbed Au nanocrystals in a certain area, for example, 300 nm by 300 nm, in the central part of the microsphere was first counted on the SEM image. The total number of the adsorbed Au nanocrystals was then calculated from the total surface area of the microsphere. The average size of the Au nanocrystals was measured from their TEM images. For their average size, we estimated the area of each nanocrystal projected onto the microsphere surface. The total surface area coverage was the product between the total number of the adsorbed nanocrystals and the projected area of each nanocrystal, and the surface area coverage percentage was the ratio between the total covered surface area and the total surface area of the microsphere.

Characterization. The measurements of the extinction spectra were performed on a Hitachi U-3501 UV−visible/NIR spectrophotometer with quartz cuvettes that have an optical path length of 0.5 cm. The SEM images were taken on an FEI Quanta 400 FEG microscope. The TEM imaging was performed on an FEI CM120 microscope at 120 kV. The scattering images and spectra of the individual microspheres were measured on a dark-field optical microscope (Olympus BX60) that was integrated with a quartz−tungsten−halogen lamp (100 W), a monochromator (Acton SpectraPro 2300i), and a charge-coupled device camera (Princeton Instruments Pixis 512B). The camera was thermoelectrically cooled to −30 °C during the measurements. An Olympus LMPlanFl dark-field objective (50×; numerical aperture, 0.50) was employed for both illuminating the microspheres with the white excitation light and collecting the scattered light. The scattered light from the individual microspheres were corrected by first subtracting the background spectra taken from the adjacent regions without microspheres and then dividing them with the calibrated response curve of the entire optical system. For the optical measurements, an aqueous HMSMS dispersion (10 μL, 0.01 mg · mL^{-1}) was deposited at the center of a glass slide that is 0.16−0.19 mm thick. A 5-mm thick PDMS block with a 1 cm × 1 cm hole at the center was placed on the glass slide. The hole with a volume of 0.5 mL was filled with water and covered with another glass slide. The entire sandwich structure was then placed on the optical stage with the slide carrying the HMSMSs

TABLE 2. Reaction Compositions for the Coating of Mesostructured Silica on the PS Microspheres

diameter (μm)/shell thickness (nm)[a]	PS microsphere size (μm)/weight (g)	ethanol (mL)	water (mL)	$NH_3 \cdot H_2O$ (28 wt %, mL)	CTAB (g)	TEOS (mL)
1.22/108	1.04/0.40	64	58	0.8	0.48	0.86
1.80/77	1.73/0.96	64	58	0.8	0.48	0.86
2.72/134	2.53/0.96	64	58	0.8	0.60	1.08

[a]The diameter and shell thickness refer to the values measured after the calcination.

facing the objective. The scattering spectra of the Au nanocrystal-decorated HMSMSs were acquired in a similar way. For the measurement of the time-dependent scattering spectra during the chemical etching process, the HMSMSs decorated with the Au nanocrystals (10 μL, 0.01 mg · mL^{-1}) were first transferred into the sandwich structure composed of two glass slides and one PDMS block. An acidic H_2O_2 solution (0.5 mL, 0.3 wt %) containing 0.05 M NaBr and 0.01 M HCl was then quickly injected into the hole at the center of the PDMS block. The measurement of the scattering spectra was conducted immediately after the injection.

Acknowledgment. This work was supported by Hong Kong RGC GRF grant (ref. No. CUHK403409, Project Code, 2160391) and Direct Allocation (Project Code, 2060393).

Supporting Information Available: The simulation details of the scattering spectra using Mie theory, SEM images of the HMSMSs and Au nanocrystal-decorated HMSMSs, TEM images of the HMSMSs, dark-field scattering image of the individual HMSMSs, scattering spectra of the PS microspheres, HMSMSs, and Au nanocrystal-decorated HMSMSs, scattering, absorption, and extinction spectra of the Au nanospheres and nanorods, and scattering spectra recorded on the individual HMSMSs during the etching process. This material is available free of charge *via* the Internet at http://pubs.acs.org.

REFERENCES AND NOTES

1. Fang, Y.; Seong, N.-H.; Dlott, D. D. Measurement of the Distribution of Site Enhancements in Surface-Enhanced Raman Scattering. *Science* **2008**, *321*, 388–392.
2. Li, J. F.; Huang, Y. F.; Ding, Y.; Yang, Z. L.; Li, S. B.; Zhou, X. S.; Fan, F. R.; Zhang, W.; Zhou, Z. Y.; Wu, D. Y.; *et al*. Shell-Isolated Nanoparticle-Enhanced Raman Spectroscopy. *Nature* **2010**, *464*, 392–395.
3. Kinkhabwala, A.; Yu, Z. F.; Fan, S. H.; Avlasevich, Y.; Müllen, K.; Moerner, W. E. Large Single-Molecule Fluorescence Enhancements Produced by a Bowtie Nanoantenna. *Nat. Photonics* **2009**, *3*, 654–657.
4. Ueno, K.; Juodkazis, S.; Mizeikis, V.; Sasaki, K.; Misawa, H. Clusters of Closely Spaced Gold Nanoparticles as a Source of Two-Photon Photoluminescence at Visible Wavelengths. *Adv. Mater.* **2008**, *20*, 26–30.
5. Sundaramurthy, A.; Schuck, P. J.; Conley, N. R.; Fromm, D. P.; Kino, G. S.; Moerner, W. E. Toward Nanometer-Scale Optical Photolithography: Utilizing the Near-Field of Bowtie Optical Nanoantennas. *Nano Lett.* **2006**, *6*, 355–360.
6. Ueno, K.; Juodkazis, S.; Shibuya, T.; Yokota, Y.; Mizeikis, V.; Sasaki, K.; Misawa, H. Nanoparticle Plasmon-Assisted Two-Photon Polymerization Induced by Incoherent Excitation Source. *J. Am. Chem. Soc.* **2008**, *130*, 6928–6929.
7. Kim, S.; Jin, J.; Kim, Y.-J.; Park, I.-Y.; Kim, Y.; Kim, S.-W. High-Harmonic Generation by Resonant Plasmon Field Enhancement. *Nature* **2008**, *453*, 757–760.
8. Schuller, J. A.; Barnard, E. S.; Cai, W. S.; Jun, Y. C.; White, J. S.; Brongersma, M. L. Plasmonics for Extreme Light Concentration and Manipulation. *Nat. Mater.* **2010**, *9*, 193–204.
9. Atwater, H. A.; Polman, A. Plasmonics for Improved Photovoltaic Devices. *Nat. Mater.* **2010**, *9*, 205–213.
10. Gurjar, R. S.; Backman, V.; Perelman, L. T.; Georgakoudi, I.; Badizadegan, K.; Itzkan, I.; Dasari, R. R.; Feld, M. S. Imaging Human Epithelial Properties with Polarized Light-Scattering Spectroscopy. *Nat. Med.* **2001**, *7*, 1245–1248.
11. Itzkan, I.; Qiu, L.; Fang, H.; Zaman, M. M.; Vitkin, E.; Ghiran, I. C.; Salahuddin, S.; Modell, M.; Andersson, C.; Kimerer, L. M.; *et al*. Confocal Light Absorption and Scattering Spectroscopic Microscopy Monitors Organelles in Live Cells with No Exogenous Labels. *Proc. Natl. Acad. Sci. U.S.A.* **2007**, *104*, 17255–17260.
12. Fang, H.; Ollero, M.; Vitkin, E.; Kimerer, L. M.; Cipolloni, P. B.; Zaman, M. M.; Freedman, S. D.; Bigio, I. J.; Itzkan, I.; Hanlon, E. B.; *et al*. Noninvasive Sizing of Subcellular Organelles with Light Scattering Spectroscopy. *IEEE J. Sel. Top. Quantum Electron.* **2003**, *9*, 267–276.
13. Perelman, L. T.; Backman, V.; Wallace, M.; Zonios, G.; Manoharan, R.; Nusrat, A.; Shields, S.; Seiler, M.; Lima, C.; Hamano, T.; *et al*. Observation of Periodic Fine Structure in Reflectance from Biological Tissue: A New Technique for Measuring Nuclear Size Distribution. *Phys. Rev. Lett.* **1998**, *80*, 627–630.
14. Backman, V.; Wallace, M. B.; Perelman, L. T.; Arendt, J. T.; Gurjar, R.; Müller, M. G.; Zhang, Q.; Zonios, G.; Kline, E.; McGillican, T.; *et al*. Detection of Preinvasive Cancer Cells. *Nature* **2000**, *406*, 35–36.
15. Mourant, J. R.; Freyer, J. P.; Hielscher, A. H.; Eick, A. A.; Shen, D.; Johnson, T. M. Mechanisms of Light Scattering from Biological Cells Relevant to Noninvasive Optical-Tissue Diagnostics. *Appl. Opt.* **1998**, *37*, 3586–3593.
16. Jory, M. J.; Cann, P. S.; Sambles, J. R.; Perkins, E. A. Surface-Plasmon-Enhanced Light Scattering from Microscopic Spheres. *Appl. Phys. Lett.* **2003**, *83*, 3006–3008.
17. Huang, L. N.; Martin, O. J. F. Distance-Controlled Scattering in a Plasmonic Trap. *Appl. Phys. Lett.* **2010**, *96*, 073104.
18. Lok, K. P.; Ober, C. K. Particle Size Control in Dispersion Polymerization of Polystyrene. *Can. J. Chem.* **1985**, *63*, 209–216.
19. Blas, H.; Save, M.; Pasetto, P.; Boissière, C.; Sanchez, C.; Charleux, B. Elaboration of Monodisperse Spherical Hollow Particles with Ordered Mesoporous Silica Shells *via* Dual Latex/Surfactant Templating: Radial Orientation of Mesopore Channels. *Langmuir* **2008**, *24*, 13132–13137.
20. Ming, T.; Zhao, L.; Yang, Z.; Chen, H. J.; Sun, L. D.; Wang, J. F.; Yan, C. H. Strong Polarization Dependence of Plasmon-Enhanced Fluorescence on Single Gold Nanorods. *Nano Lett.* **2009**, *9*, 3896–3903.
21. Sinzig, J.; Quinten, M. Scattering and Absorption by Spherical Multilayer Particles. *Appl. Phys. A: Mater. Sci. Process.* **1994**, *58*, 157–162.
22. Lankers, M.; Khaled, E. E. M.; Popp, J.; Rössling, G.; Stahl, H.; Kiefer, W. Determination of Size Changes of Optically Trapped Gas Bubbles by Elastic Light Backscattering. *Appl. Opt.* **1997**, *36*, 1638–1643.
23. Liu, Y.; Li, X.; Kim, Y. L.; Backman, V. Elastic Backscattering Spectroscopic Microscopy. *Opt. Lett.* **2005**, *30*, 2445–2447.
24. Ni, W. H.; Kou, X. S.; Yang, Z.; Wang, J. F. Tailoring Longitudinal Surface Plasmon Wavelengths, Scattering and Absorption Cross Sections of Gold Nanorods. *ACS Nano* **2008**, *2*, 677–686.
25. Tsung, C.-K.; Kou, X. S.; Shi, Q. H.; Zhang, J. P.; Yeung, M. H.; Wang, J. F.; Stucky, G. D. Selective Shortening of Single-Crystalline Gold Nanorods by Mild Oxidation. *J. Am. Chem. Soc.* **2006**, *128*, 5352–5353.
26. Frens, G. Controlled Nucleation for the Regulation of the Particle Size in Monodisperse Gold Suspensions. *Nature (London), Phys. Sci.* **1973**, *241*, 20–22.
27. Glogowski, E.; Tangirala, R.; He, J. B.; Russell, T. P.; Emrick, T. Microcapsules of PEGylated Gold Nanoparticles Prepared by Fluid−Fluid Interfacial Assembly. *Nano Lett.* **2007**, *7*, 389–393.
28. Kou, X. S.; Ni, W. H.; Tsung, C.-K.; Chan, K.; Lin, H.-Q.; Stucky, G. D.; Wang, J. F. Growth of Gold Bipyramids with Improved Yield and Their Curvature-Directed Oxidation. *Small* **2007**, *3*, 2103–2113.